Analytical Model of Pulsing of Solid Propellant Rocket Motors

R.M. Hackett*
The University of Alabama in Huntsville, Huntsville, Alabama

and

C.E. DeVilbiss†
John W. McDougall Company, Inc., Nashville, Tennessee

The finite-element formulations of structural and acoustic free-vibration problems are reviewed and compared, and the mode superposition analysis technique is presented. A direct analogy is developed between the application of mode superposition to combustion instability analysis, and its proven application in structural analysis. A computer program which models the response of pulsed solid propellant rocket motor cavities is presented, and examples that demonstrate the application of the program are discussed.

Nomenclature

$( )$	= function of enclosed variable(s)
$\{ \}$	= column vector
$[ ]$	= row vector
$[ ]$	= rectangular or square matrix
$[ ]^T$	= transpose of a matrix
$[ ]^{-1}$	= inverse of a square matrix
$[ ]^{-T}$	= inverse of the transpose of a square matrix
$\bar{( )}$	= indicates transformed matrix when placed over a symbol
$\tilde{( )}$	= indicates transformed quantity when placed over a symbol
a, b	= arbitrary proportionality constants
$\{A\}, \{a\}$	= field value vectors
B	= fluid bulk modulus
$[B]$	= matrix relating strains to displacements
C	= element of the diagonalized damping matrix
$[C], [c]$	= damping matrices
$[D]$	= matrix relating stresses to strains
e	= exponential
$\{f\}$	= forcing function vector
$[F], [f]$	= fluid "equivalent potential energy" matrices
$[G], [g]$	= fluid "equivalent kinetic energy" matrices
H	= energy functional
$[I]$	= identity matrix
$[K], [k]$	= stiffness matrices
$[L]$	= lower triangular matrix
$[M], [m]$	= mass matrices
$[N]$	= matrix of shape functions
p	= pressure
$\{Q\}, \{q\}$	= perturbation vectors
$[R]$	= matrix operator
t	= time
$[T]$	= transformation matrix
u	= displacement
$\{u\}$	= displacement vector
V	= volume
$\{x\}$	= coordinate vector
x, y, z	= rectangular Cartesian coordinates
X	= generalized coordinate
α	= growth/decay constant
ζ, η	= integration constants
λ	= eigenvalue
μ	= viscosity function
ξ	= damping ratio
ρ	= mass density
$[\Phi]$	= set of n orthogonal base vectors
$\{\phi\}$	= mode shape vector
$[\Omega^2]$	= matrix of eigenvalues
ω	= natural circular frequency

Superscript

e	= element

Subscripts

i	= mode
$i, j, \ldots, m$	= element nodal point numbers
k	= kinetic energy
n	= number of discrete variables; nth condition
p	= potential energy
r, s	= mode designations
o	= initial condition

Introduction

THE pulsing of a solid propellant rocket motor is a means of examining the behavior of the motor during its combustion. The combustion process has been observed to produce within the rocket motor cavity pressure oscillations which correspond to the natural acoustic modes of vibration of the cavity.[1] These natural acoustic modes are the acoustic free-vibration modes of the cavity and may be thought of as being similar to acoustic vibrations in organ pipes. When the combustion process excites one or more of the natural modes of the motor to the extent that cavity pressure oscillations continuously increase in amplitude, a condition of combustion instability may exist. By physically pulsing a burning rocket motor and measuring the resultant pressure oscillations, data pertinent to combustion instability prediction are gathered.[2] Previous analytical work[3] has consisted of the formulation of ballistic models for three different types of laboratory pulser units and the modification of a nonlinear finite difference combustion instability program to model the effect of fore-end pulsing, based on mass and energy flux data provided by the pulser ballistic analyses. A computational model of the pulsing process which could be coupled with a finite-element combustion instability prediction capability would enhance experimental projects by providing a means of optimizing data

Received Sept. 2, 1983; revision received Jan. 24, 1984.

*Professor of Civil Engineering.

†Project Engineer.

collection (e.g., pulse and pressure measurement locations to best observe certain modes), and would provide a link between experimental pulse work and analytical prediction.

Toward the practical solution of the problem of combustion instability prediction, much effort has been expended on the development of closed-form stability integrals based on linear combustion theory. These stability integrals make use of the solid rocket motor cavity natural acoustic modes. Determination of the natural mode frequencies and mode pressure distributions, or mode shapes, has become quite complicated due to the complex configuration of modern solid propellant rocket motor cavities. Consequently, numerical approximation, in the form of the finite-element method, was adopted in 1975 as the standard means of extracting natural acoustic vibration frequencies and mode shapes for solid propellant rocket motors.[4]

The finite-element method is a numerical approximation procedure through which, by discretizing a function, such as the continuous pressure function mentioned above, it is possible to describe approximately the variation of that function throughout a continuum by the numerical value of the function at specific points. This can be easily visualized as a process similar to graphing an arbitrary function $y=f(x)$ by plotting values of y at specific values of x. If discrete variables are assigned to the function's numerical value at the specific points and assumptions are made about the variation of the function between points, it is possible to write a set of simultaneous equations in terms of these discrete variables. The equations arise from a superpositioning of equations written for each "finite element" (continuum subregion) bounded by the nodal points chosen as above. Equations on the element level are commonly generated by energy balance relationships, which are based on the physical properties of the finite element of continuum material. Thus, the finite-element method consists of discretizing a continuous function and superposing equations developed at the element level.[5] In general, finite-element accuracy is directly proportional to the number of elements used.

Formulation for the finite-element approximation of the acoustic free-vibration problem results in a mathematical phenomenon known as the general eigensystem[6]:

$$[F]\{\phi\}=\lambda[G]\{\phi\} \tag{1}$$

where the matrices $[F]$ and $[G]$ are determined by the physical properties of the system, λ is an unknown constant, and the vector $\{\phi\}$ represents the discrete variables of the finite-element formulation. Solution of the general eigensystem results in eigenpairs

$$(\lambda_i,\{\phi_i\}), \qquad i=1,2,\ldots,n \tag{2}$$

where n is the number of discrete variables. Each eigenpair represents an eigenvalue, (frequency)^2, λ_i, and eigenvector mode shape, $\{\phi_i\}$, which describe a natural mode of acoustic vibration.

Modeling of the dynamic response of a rocket motor cavity to pulse perturbations will be approached within the finite-element framework. This is accomplished by the application of mode superposition, a technique commonly employed in structural engineering vibration analyses.[7,8] Conceptually, mode superposition is a procedure whereby the response of an entire continuum is found by superposing the responses within some or all of the natural modes. The number of modal responses used depends on the accuracy sought and the characteristics of the natural modes, in that some may affect the total response more than others. Two aspects of mode superposition make it very attractive for this pulse modeling problem. First, it is founded on the solution of the eigensystem, which is necessary for linear combustion instability analysis. Secondly, the individual modal responses are generated, which is advantageous because frequently only a few modes exhibit combustion instability tendencies, and the ability to examine these modes separately is of obvious merit. Therefore, mode superposition as an extension of the finite-element method in combustion instability analysis will be used to model rocket motor cavity response to a short duration pressure increase applied at one or more of the cavity nodal points as a pulse perturbation, with the resulting pressure oscillations throughout the cavity calculated by solving the differential equations of dynamic equilibrium in time.

Background

Combustion Instability

Combustion instability, as used herein, refers to the behavior of an oscillating rocket motor cavity when the combustion process drives the pressure oscillations to such an extent that detrimental effects result on the rocket flight. Such effects can include: malfunction of electronic guidance equipment, failure of mechanical components, disturbance of the combustion process itself, or unsatisfactory vibration of delicate cargo, e.g., passengers. The onset and maturity of combustion instability result from either the inherent acoustic instability of a specific combination of cavity geometry and propellant grain composition or the amplification of a cavity pressure disturbance by the combustion process itself. A rocket motor may be unstable in one or more of the acoustic modes, or it may be marginally stable, thereby becoming unstable with sufficient perturbation. As the complexity of the cavity geometry increases, so does the likelihood that more than one acoustic mode antinode will occur at a given point. This superpositioning of antinodes can have the effect of large variations in pressure on the cavity surface.

The combustion process is obviously highly complex. As a rocket motor burns, not only are the pressure, density, and temperature of the cavity gases constantly changing, but with propellant combustion there is also a change in cavity shape which produces changes in the acoustic modes. These changes result in varying combustion rates, and the cycle goes on. The combustion process can attenuate the acoustic waves as well as amplify them. In addition, several other phenomena are known to drive or damp the pressure oscillations, some the result of cavity gas flow effects, others of a purely mechanical nature. Combustion instability occurs when the net result of all factors produces an amplified acoustic wave which grows beyond a suitable limit as the rocket motor burns. Prediction of the combustion instability phenomenon is a problem of evaluating this net influence on the pressure waves of each of the natural acoustic modes of the cavity.

A simple analytical model of the combustion instability problem within a single acoustic mode is[9]:

$$p=p_0e^{\alpha t}\cos\omega t \tag{3}$$

where p_0 is the amplitude of the disturbance and α the net exponential rate of change of the disturbance. Accurate determination of the parameter α is the objective of a combustion instability analysis, a positive α indicating growth of the pressure disturbance and consequent instability, and a negative α indicating decay of the disturbance, or stability. The α parameter of Eq. (3) is the stability indication of a single mode of acoustic vibration, hence it is possible for a rocket motor to be stable in all but one acoustic mode. Much work has been expended toward the goal of analytical prediction of instability, but much is yet to be done. Advancement of theory and analytical procedures is linked closely to experimental results obtained from laboratory tests and telemetry data from actual rocket motor firings. One such laboratory test is cavity pulsing, which is valuable in experimental determination of the growth/decay parameter.

Solid Propellant Rocket Motor Pulsing

Pulsing methods to evaluate the combustion instability characteristics of solid rocket motors experimentally have

been employed since the mid-1960's.[2] In essence, the technique consists of firing a pressure pulse into a burning rocket motor and then recording the induced pressure oscillations. Immediately after the motor burns out, a second pulse is introduced and a similar pressure response recorded. Analysis of the data is then carried out in the time domain and electronic filtering is applied to determine the frequency content.

Time domain analysis consists merely of determining the peak to peak pressure oscillation amplitude change. This growth/decay factor of pressure amplitude is the α parameter. Using the definition of disturbance propagation, Eq. (3)

$$p_n = p_0 e^{\alpha t_n} \cos \omega t_n \tag{3a}$$

where n corresponds to the number of cycles considered. Thus α is evaluated by measuring peak amplitudes in the time domain and solving the simple equation:

$$\alpha = \ell n(p_n/p_0)/t_n \tag{4}$$

Such an analysis of the first record yields the growth/decay parameter during combustion. A similar analysis of the second record yields growth/decay information attributable to the combustion gases alone. From a comparison of the values, not only is stability or instability evident, but information about the acoustic energy production of the combustion process is also attainable, since the net effect of combustion is determined from the difference between the two records.

Frequency domain analysis of the pressure oscillation records is conducted by feeding the data through a spectral frequency analyzer. Such an analysis yields a breakdown of the frequency, or acoustic mode composition of the record. These data are valuable in checking analytical model mode predictions which produce frequencies and mode pressure distributions, although only the frequencies can be compared, as mode shapes are unattainable from pulse experimentation.

The growth/decay parameters determined in the time domain analysis are for the combination of all the modes excited by the pulse and recorded by the pressure transducers. It is only possible to extract specific mode decay factors through electronic filtering devices, which distort the data and introduce error. Therefore it is essential to conduct a coordinated analysis of experimental data and analytical results to fully gain the benefits of pulsing technology.[10]

Application of pulse testing to a rocket motor is carried out by attaching accelerometers to the motor casing and tapping pressure sensitive transducers into the rocket motor cavity. Pulses are injected into the burning cavity, either by piston type plungers or by explosive charge. Orientation of the pulser is significant in that longitudinal modes are excited by any pulse, whereas tangential modes of the cavity tend to receive more energy from the pulse when it is fired into the cavity in an asymmetrical, off-axis fashion.[2]

Finite-Element Method

Since the early 1960's, when the finite-element method received its formal name from a structural analysis application, it has evolved into a highly mathematically developed numerical approximation technique which is applicable to a diverse family of physical problems—structural analysis, electrical circuitry, fluid flow, heat conduction.

Finite-element analysis techniques are applicable to linear problems, and to nonlinear problems through the concepts of linearization and iteration. However, the following discussion will be confined to linear applications, as the presently most tractable combustion instability prediction theory is linear. The actual solution of a finite-element problem can be summarized as consisting of four steps. First, the continuous domain of the system is broken into subregions, or finite elements, and element properties are generated from geometric, material, and loading conditions which are assumed well defined and specified. Second, all elemental subregions are assembled into a discretized formulation of the continuous problem. Third, boundary conditions are imposed on the system of generated equations. Fourth, the equations are solved to produce output data, which is the desired result.

Discretization of a continuous problem is accomplished by dividing the domain of concern into finite-element subregions defined geometrically through the coordinates of boundary points, or nodes. Then the continuous field of interest, e.g., temperature, pressure, displacement, etc., is defined in terms of its value at these nodal points. Continuity of the field is preserved by assuming a set of shape functions for each finite element which expresses the value of the field at the element nodal points. These shape functions are an approximation introduced into the formulation in that they are rarely assumed to be higher than second order, whereas the field variation is unknown. Thus

$$\{a\} = \Sigma [N_i]\{a_i\}^e = [N_i, N_j, \ldots, N_m] \begin{Bmatrix} a_i^e \\ a_j^e \\ \vdots \\ a_m^e \end{Bmatrix} = [N]\{a\}^e \tag{5}$$

defines $\{a\}$ at some point in terms of the shape functions $[N_i]$ for nodal points $i = 1, 2, \ldots, m$, m being the number of nodal points per element, and the field values at the nodal points $\{a_i\}^e$. The shape functions are functions which map the nodal values into values at interior points in the element, consequently the coordinates of the point where $\{a\}$ is defined are expressed as

$$\{x\} = [N]\{x\}^e \tag{6}$$

and the property of identity mapping at the nodal points becomes apparent,

$$\{x_i\} = [N_i]\{x_i\} \quad \text{or} \quad [N_i] = N_i[I] \tag{7}$$

if all components of the $\{x\}^e$ vector are mapped identically.

Material properties are introduced to establish a relationship between the field of interest $\{a\}$ and some perturbing function which will be called $\{q\}$. Physical considerations between the field and its perturbation on the element level may take the form of displacement-force in structural problems, current-voltage in electrical problems, etc., and are expressed discretely as

$$\{q\}^e = [k]^e \{a\}^e \tag{8}$$

where $[k]^e$ will be referred to as the element stiffness matrix, which is the terminology used in structural problems. The vector $\{q\}^e$ represents nodal perturbation values associated with the nodal field values; consequently, it has the same number of components as $\{a\}^e$, and $[k]^e$ is seen to be square. Many linear problems induce symmetry into $[k]^e$ through reciprocity.

With the problem discretized and elemental equations formulated by introduction of the material properties associated with the system, the first step in the finite-element solution is completed, so the second step, assembly, is undertaken. By noting the continuity constraint at nodal points, which requires element nodal point displacements to be the same for any elements sharing that nodal point, the property of simple additivity is seen to govern the assembly process. In essence, the elements surrounding a nodal point all have material property influence on the field value at that node, thus the element equations are simply summed to give discrete global equations of the form

$$[Q] = \sum \{q\}^e = \sum [k]^e \{a\}^e = [K]\{A\} \tag{9}$$

Equation (9) is constrained only in the continuity relationship imposed at the nodal points of the finite elements; therefore, the third step in formulating the problem is to impose boundary conditions on the discrete field variables in $\{A\}$. This consists merely of restraining the field values at any nodes which have imposed conditions. An example is specified displacement values at support points in a structural analysis problem.

All that remains is the solution of Eq. (9) with the imposed boundary conditions to yield a field vector $\{A\}$, the discrete values to the continuous field associated with the perturbation vector $\{Q\}$. As previously noted, the global stiffness matrix is normally symmetric, which enhances solution of the equations. Another enhancing feature arises due to the "mesh" which results from dividing the domain through the introduction of nodal points. Continuity constraints couple the global equations only at nodal points shared by elements; consequently, the global stiffness matrix is sparsely filled with band widths on the order of 10% of the total number of equations. So, even though finite-element discretization leads to a large system of simultaneous equations, they are typically "nice" equations which are relatively easily solved.

Discretization, assembly, constraint, and solution are the four steps common to the general finite-element problem regardless of application. The only approximation introduced in the formulation is assumption of the shape functions, which approximate the variation of element parameters throughout the finite-element subregion. Other approximations may be introduced in the material property relationships (commonly defined as integral quantities which must be evaluated numerically), and the equation solution step. However the shape function approximation is usually the dominant factor, so as the shape functions represent the actual variation of element parameters more closely, accuracy improves. Better shape function approximation can be achieved by one of two methods: 1) increase the order of the shape functions assumed or 2) decrease the variation of parameters between nodal points by defining more of them, and, hence, more elements. The second option of refining the finite-element mesh is usually chosen when more accuracy is necessary, accuracy being related directly to the number of elements chosen to discretize the problem domain.

Equation (9) was formulated based on a general perturbation function $\{Q\}$. Time may now be introduced by allowing the perturbation to include contributions which depend on time rates of change of the field vector, denoted:

$$\{\dot{A}\} = \frac{\mathrm{d}}{\mathrm{d}t}\{A\} \quad \text{and} \quad \{\ddot{A}\} = \frac{\mathrm{d}}{\mathrm{d}t}\{\dot{A}\} \tag{10}$$

Recalling that the concept of discretization, Eq. (5), was applied to the spatial domain of the problem, it is clear that just as $[k]^e$ related the field variables to perturbation for the finite element, so should exist discrete matrices relating the rates of change, Eq. (10), to perturbation on the element level. Such is the case, and Eq. (8) may now be written as

$$\{q\}^e = [k]^e\{a\}^e + [c]^e\{\dot{a}\}^e + [m]^e\{\ddot{a}\}^e \tag{11}$$

and, upon assembly as before,[5,7,8]

$$\{Q\} = [K]\{A\} + [C]\{\dot{A}\} + [M]\{\ddot{A}\} \tag{12}$$

which is the general discrete form of the equations of dynamic balance between perturbations and the values of the field of interest and its time derivatives. Returning to the example of structural analysis, wherein perturbations are forces and the field is of displacements, $[C]$ is referred to as the global damping matrix, and $[M]$ is referred to as the global mass matrix. Damping force contributions are of a viscous nature, or velocity-dependent, and mass forces are inertia related, or acceleration-dependent.

Referring once again to the structural problem, the general forms of matrices $[k]^e$, $[c]^e$, and $[m]^e$ are defined in the following manner[5]:

$$[k]^e = \int_{V^e} [B]^T [D][B]\,\mathrm{d}V^e \tag{13}$$

where $[B]$ is comprised of partial derivatives of the shape functions:

$$[B] = \left[[B_i], [B_j], \ldots, [B_m]\right] \tag{14}$$

$i, j, \ldots, m$ being the element nodal points, and for the three-dimensional case,

$$[B_i]^T = \begin{bmatrix} \frac{\partial N_i}{\partial x} & 0 & 0 & \frac{\partial N_i}{\partial y} & 0 & \frac{\partial N_i}{\partial z} \\ 0 & \frac{\partial N_i}{\partial y} & 0 & \frac{\partial N_i}{\partial x} & \frac{\partial N_i}{\partial z} & 0 \\ 0 & 0 & \frac{\partial N_i}{\partial z} & 0 & \frac{\partial N_i}{\partial y} & \frac{\partial N_i}{\partial x} \end{bmatrix}, \text{ etc.} \tag{15}$$

matrix $[D]$ of Eq. (13) is a matrix of constitutive properties relating stress and strain;

$$[c]^e = \int_{V^e} [N]^T \mu [N]\,\mathrm{d}V^e \tag{16}$$

$$[m]^e = \int_{V^e} [N]^T \rho [N]\,\mathrm{d}V^e \tag{17}$$

Thus the general discrete equations of dynamic balance, Eq. (12), which result from discretization of a continuous domain, are established. The solution of these equations is more complicated in that they must be solved in time, but, in general, a dynamic finite-element analysis problem can be readily solved.

Motivation for turning to the finite-element method in combustion instability analysis comes from the need to extract natural acoustic vibration frequencies and mode shapes for complex rocket motor configurations.[11] The presence of slots or other cutouts in the propellant grain make determination of the natural frequencies virtually impossible by methods of classical acoustic analysis. By discretizing the system through the finite-element method, numerical evaluation of the modes is possible.

Once the finite-element method gained acceptance in combustion instability analysis, it became apparent that a standardized procedure for acoustic analysis would be beneficial.[4] The finite-element code, NASTRAN (NASA STRuctural ANalysis), was adopted for that purpose.[4,11] As is obvious from its name, NASTRAN is a structural finite-element code; however, it contains a fluid analysis capability, and this option was utilized to extract natural frequencies and mode shapes. A post-processor was then employed to carry out a potential flow analysis and combustion instability prediction.

Because NASTRAN was not designed as a combustion instability analysis program, it has inconvenient aspects. Some of these are: 1) an axisymmetric, rather than three-dimensional, analysis, 2) approximation of the cavity slots, accuracy of which decreases as slot width increases, 3) inability to couple the acoustic response of the rocket motor cavity to the structural response of the propellant grain, and 4) requirement of a post-processor to predict instability. These drawbacks led to the conclusion that a program designed solely for combustion instability analysis would be much more useful.[12] Subsequent effort resulted in the development of FLAP3 (FLuid Analysis Program, 3-Dimensional).[13] The FLAP3 code is important to this work, because results from

the code are used as input for the analytical pulse code, which will be demonstrated subsequently. For this reason, a brief description of the capabilities of FLAP3 will be given. It was designed to perform a linear acousto-modal analysis of the irrotational motions of an inviscid, compressible fluid coupled to the motions of a nearly incompressible, linearly viscoelastic solid, and a linear potential flow analysis of the irrotational motions of an inviscid, incompressible fluid, and then determine the effect of the flowfield and combustion on the acoustic oscillations of the rocket motor. The development of this three-dimensional code was motivated primarily by three objectives: 1) to provide more generality in modeling complex cavity geometries, 2) to provide a means of predicting the damping of acoustic oscillations by the solid propellant grain, and 3) to provide an easy-to-use, integrated program designed solely for the purpose of combustion instability prediction.[13] It has been shown that FLAP3 produces analytic results which are in good agreement with experimental data.[14]

Theory

Structural Analogy

It will now be shown that structural dynamics problems are analogous in theoretical formulation to the problem of the dynamic response of solid propellant rocket motors and that the solution procedures can be virtually identical within certain limitations. Discretization of the fluid flow problem in rocket motor cavities is based on an Eulerian kinematic assumption. Simply stated, the finite elements are assumed to represent subregions of the domain through which the fluid flows, with fluid pressure at the nodal points being the discrete values of the field sought.[15] Thus the nodal points of the finite element mesh remain stationary. In comparison, this differs from the common formulation of structural problems, which is based on a Lagrangian kinematic assumption. Finite elements in a solid structure are taken as subregions of the material with the actual displacement of the nodal points being the discrete field values.[5,8] These displacements are related to actual deformations of the finite-element mesh. However, regardless of this kinematic assumption difference, the discrete set of equations which result from either formulation will be of the same structure.

Finite-element formulation of the acoustic free vibration problem will be approached as the minimization of an energy functional, H, which is composed of potential energy and kinetic energy contributions:[12]

$$H = H_p + H_k \tag{18}$$

The potential energy term is defined as

$$H_p = \frac{1}{2}\int_V \frac{1}{\rho}\left\{\left(\frac{\partial p}{\partial x}\right)^2 + \left(\frac{\partial p}{\partial y}\right)^2 + \left(\frac{\partial p}{\partial z}\right)^2\right\} \mathrm{d}V \tag{19}$$

where the bracketed term is the vector inner product of the spatial pressure gradient with itself. The kinetic energy is defined as

$$H_k = -\frac{1}{2}\int_V \frac{1}{B}\omega^2 p^2 \,\mathrm{d}V \tag{20}$$

Minimization of the energy functional, Eq. (18), is equivalent to requiring

$$\frac{\partial H}{\partial p} = \frac{\partial H_p}{\partial p} + \frac{\partial H_k}{\partial p} = 0 \tag{21}$$

Discretization of the problem is begun by introducing the standard shape function approximation, Eq. (5), to give

$$p(x, y, z) = \lfloor N \rfloor \{ p \}^e \tag{22}$$

where

$$\lfloor p \rfloor^e = \lfloor p_i, p_j, \ldots, p_m \rfloor \tag{23}$$

Now, on the element level

$$\frac{\partial H_p}{\partial p^e} = \left\lfloor \frac{\partial H_p}{\partial p_i} \cdots \frac{\partial H_p}{\partial p_m} \right\rfloor^e \tag{24}$$

where, from Eq. (19) it is seen that

$$\frac{\partial H_p}{\partial p_i} = \int_{V^e} \frac{1}{\rho}\left\{\left(\frac{\partial p}{\partial x}\right)\frac{\partial}{\partial p_i}\left(\frac{\partial p}{\partial x}\right) + \left(\frac{\partial p}{\partial y}\right)\frac{\partial}{\partial p_i}\left(\frac{\partial p}{\partial y}\right) + \left(\frac{\partial p}{\partial z}\right)\frac{\partial}{\partial p_i}\left(\frac{\partial p}{\partial z}\right)\right\} \mathrm{d}V^e, \text{ etc.} \tag{25}$$

and a matrix $[f]^e$ can be defined such that

$$\frac{\partial H_p}{\partial p^e} = [f]^e \{ p \}^e \tag{26}$$

with a typical term of $[f]^e$ expressed as

$$f^e_{rs} = \int_{V^e} \frac{1}{\rho}\left(\frac{\partial N_r}{\partial x}\right)\left(\frac{\partial N_s}{\partial x}\right) + \left(\frac{\partial N_r}{\partial y}\right)\left(\frac{\partial N_s}{\partial y}\right) + \left(\frac{\partial N_r}{\partial z}\right)\left(\frac{\partial N_s}{\partial z}\right) \mathrm{d}V^e \tag{27}$$

where $r, s = i, j, \ldots, m$. Similarly

$$\frac{\partial H_k}{\partial p^e} = \left\lfloor \frac{\partial H_k}{\partial p_i} \cdots \frac{\partial H_k}{\partial p_m} \right\rfloor^e \tag{28}$$

where from Eq. (20) it is seen that

$$\frac{\partial H_k}{\partial p_i} = -\int_{V^e}\left(\frac{1}{B}\omega^2 p \frac{\partial p}{\partial p_i}\right) \mathrm{d}V^e, \text{ etc.} \tag{29}$$

By letting

$$\frac{\partial H_k}{\partial p^e} = -\omega^2 [g]^e \{ p \}^e \tag{30}$$

it is seen that another element matrix $[g]^e$ is defined by

$$g^e_{rs} = \int_{V^e} \frac{1}{B}(N_r N_s) \,\mathrm{d}V^e \tag{31}$$

Recalling that finite-element assembly requires merely direct summation over all elements, it is clear that

$$\frac{\partial H}{\partial p} = \sum \frac{\partial H^e}{\partial p^e} = 0 \tag{32}$$

Thus, the final formulation of the discretized acoustic free-vibration problem is:

$$[F]\{ p \} = \omega^2 [G]\{ p \} \tag{33}$$

Both global matrices are symmetric, as is obvious from the definitions of the element matrices, Eqs. (27) and (31).

To compare the acoustic free-vibration equations, Eq. (33), to those of the structural free-vibration problem, it is sufficient to write the general dynamic equations in terms of force and displacement:

$$[M]\{ \ddot{u} \} + [C]\{ \dot{u} \} + [K]\{ u \} = \{ f(t) \} \tag{34}$$

and then to disregard the viscous and forcing terms, which

yields

$$[M]\{\ddot{u}\}+[K]\{u\}=0 \tag{35}$$

Taking

$$\{u\}=\{\phi\}e^{i\omega t} \tag{36}$$

and substituting this expression into Eq. (35) yields

$$[K]\{\phi\}=\omega^2[M]\{\phi\} \tag{37}$$

which is clearly similar to Eq. (33). Thus the discretized free-vibration problem in acoustics and structures yields essentially the same set of equations. So similar are the formulations that it has been shown that a structural analysis computer code can actually yield the correct solution for an acoustic problem from appropriately altered input data.[15]

Eigenvalue Solution

A large number of mathematical models of physical systems can be reduced to the solution of a special eigenvalue problem defined by the eigensystem:[5]

$$[R]\{x\}=\lambda\{x\} \tag{38}$$

Solution of the free-vibration equations, Eqs. (33) and (37), of acoustic vibration and structural vibration, respectively, can be reduced to that of the special eigensystem, Eq. (38). As an example of the procedure utilized to reduce the vibration equations, such a reduction will be applied to the structural free-vibration equations. Matrices $[K]$ and $[M]$ are known to be symmetric by definition, so maintenance of symmetry is sought in their combination to produce a matrix $[R]$ for Eq. (38). This is accomplished by constructing a triangular decomposition of $[K]$ such that

$$[K]=[L][L]^T \quad \text{and} \quad [K]^{-1}=[L]^{-T}[L]^{-1} \tag{39}$$

Substituting Eq. (39) into Eq. (37), premultiplying by $[L]^T$, and then rearranging yields

$$[L]^{-1}[M]\{\phi\}=\lambda[L]^T\{\phi\} \tag{40}$$

where $\lambda=1/\omega^2$. Setting

$$[L]^T\{\phi\}=\{x\} \tag{41}$$

the reduction is complete, and

$$[R]\{x\}=\lambda\{x\} \tag{42}$$

where

$$[R]=[L]^{-1}[M][L]^{-T} \tag{43}$$

The solution of Eq. (42) is a well-understood mathematical exercise and many standard computer algorithms exist for the extraction of eigenvalues and eigenvectors, so it is seen that the free-vibration problems are highly solvable.

The free-vibration eigensolution yields eigenpairs

$$(\omega_1,\{\phi_1\}),(\omega_2,\{\phi_2\}),\ldots,(\omega_n,\{\phi_n\}) \tag{44}$$

where n is the number of discretized equations or the dimension of the square matrices $[K]$ and $[M]$, or $[F]$ and $[G]$. Eigenvalue ω_i, $i=1,\ldots,n$, represents the free-vibration frequency of a single mode of vibration and $\{\phi_i\}$, $i=1,\ldots,n$, which is determined to within an arbitrary multiplicative constant, represents the shape of the vibratory mode defined by the eigenvalue. The eigenvectors of Exp. (44) form an orthogonal basis for the space of solutions to the general discrete dynamic balance Eq. (12) and, as such, exhibit the properties[5,8]

$$[\phi_r][M]\{\phi_s\}=0$$

$$[\phi_r][K]\{\phi_s\}=0 \qquad (r\neq s) \tag{45}$$

If, as the magnitude of $\{\phi_r\}$ is arbitrary, the condition

$$[\phi_r][M]\{\phi_r\}=1 \tag{46}$$

is imposed on the eigenvectors, they now form an $[M]$-orthonormal basis and it is apparent that

$$[\phi_r][K]\{\phi_r\}=\omega_r^2, \qquad r=1,2,\ldots,n \tag{47}$$

Such normalization is commonly utilized in structural vibration problems. Its merit will become apparent in the following section, where mode superposition is employed as the theoretical basis for the analytical pulsing of rocket motors.

Mode Superposition

It has been shown that finite-element discretization of continuous dynamic problems often leads to the general discrete form of the equations of dynamic balance, which represent a large system of coupled equations. Solution of such a system is typically accomplished by computing values for the field and its time derivatives at discrete time intervals; the solution at some point in time depending on the values of the previous time interval, the perturbation at the current time, and satisfaction of the balance equations at the current time. As the direct solution of Eq. (12) requires solution of a large number of coupled equations at each time interval, it is a formidable computational task. Reduction of the degree-of-coupling of the equations, or optimally, uncoupling of the equations, would greatly enhance the solution by reducing computational effort. Mode superposition is a technique whereby the coupled equations of dynamic balance are uncoupled into single-degree-of-freedom equations representing the response of the system in each of its natural vibration modes, then the total response is obtained by superpositioning the modal responses.

Referring once again to the dynamic balance equations for structural problems for this discussion, Eq. (34) is seen to be the governing set of equations. Uncoupling of the equations is approached by assuming the displacements, $\{u\}$, to be expressable in terms of a transformation of some generalized modal coordinates, $\{X\}$,[8]

$$\{u\}=[T]\{X\} \tag{48}$$

where $[T]$ is some transformation matrix. Substitution of Eq. (48) into Eq. (34) and premultiplication by $[T]^T$ yields

$$[\bar{M}]\{\ddot{X}\}+[\bar{C}]\{\dot{X}\}+[\bar{K}]\{X\}=\{\bar{f}\} \tag{49}$$

where

$$[\bar{M}]=[T]^T[M][T] \tag{50a}$$

$$[\bar{C}]=[T]^T[C][T] \tag{50b}$$

$$[\bar{K}]=[T]^T[K][T] \tag{50c}$$

$$\{\bar{f}\}=[T]^T\{f(t)\} \tag{50d}$$

Judicious choice of $[T]$ will reduce the bandwidth of the equations, the optimum result being diagonal matrices $[\bar{M}]$, $[\bar{C}]$, and $[\bar{K}]$, thereby reducing the system to a set of uncoupled equations.

It can be recalled that the eigenvectors defined in the previous section form an orthogonal basis for the solution space. Thus by choosing $[T]$ to be the $n\times n$ square matrix

comprised of the eigenvectors,

$$[T] = [\{\phi_1\}\{\phi_2\}\cdots\{\phi_n\}] = [\Phi] \tag{51}$$

the original transformation becomes

$$\{u\} = [\Phi]\{X\} \tag{52}$$

and Eq. (49) may now be written as

$$[I]\{\ddot{X}\} + [\bar{C}]\{\dot{X}\} + [\Omega^2]\{X\} = \{\bar{f}\} \tag{53}$$

where $[I]$ is the identity matrix,

$$[\bar{C}] = [\Phi]^T[C][\Phi] \tag{54a}$$

$$[\Omega^2] = \begin{bmatrix} \omega_1^2 & & & \\ & \omega_2^2 & & 0 \\ & & \ddots & \\ & 0 & & \\ & & & \omega_n^2 \end{bmatrix} \tag{54b}$$

$$\{\bar{f}\} = [\Phi]^T\{f(t)\} \tag{54c}$$

Thus, with the exception of $[\bar{C}]$, Eq. (53) is uncoupled by the diagonality of $[I]$ and $[\Omega^2]$. If the original damping matrix $[C]$ is assumed to be a linear combination of $[K]$ and $[M]$ such that

$$[C] = a[M] + b[K] \tag{55}$$

then $[\Phi]$ will be orthogonal to $[C]$, and $[\bar{C}]$ will be diagonalized. Such an assumption is commonly used and is referred to as Rayleigh damping; its applicability will be discussed subsequently.

Assuming Rayleigh damping, Eq. (53) is completely uncoupled and may be written as n single-degree-of-freedom equations of the form[8]:

$$\ddot{X}_r + C_r\dot{X}_r + \omega_r^2 X_r = \tilde{f}_r \tag{56}$$

where C_r represents an element of the diagonalized damping matrix $[\bar{C}]$, ω_r is the frequency of the rth natural mode, X_r is the generalized coordinate which represents the response of the rth mode, and $\tilde{f}_r$ is the modal forcing function defined by

$$\tilde{f}_r = \lfloor \phi_r \rfloor \{f(t)\} \tag{57}$$

$\lfloor \phi_r \rfloor$ being the rth eigenvector mode shape. The solution of Eq. (56) in time gives the generalized coordinate $X_r(t)$ for each natural mode of vibration. The actual response of the system is then achieved by transforming the generalized response, as in Eq. (52)

$$\{u_r(t)\} = X_r(t)\{\phi_r\} \tag{58}$$

where $\{u_r(t)\}$ is the actual displacement of the system in the rth natural mode of vibration.

As mentioned previously, $[\Phi]$ represents a set of n orthogonal base vectors for the solution space in which $\{u\}$, the total response, exists. Therefore any solution $\{u\}$ may be thought of as a linear combination of the base vectors $\{\phi_r\}$. This is equivalent to recognizing that the total response is a combination of vibrations in each of the system's natural modes. The concept of superposition is introduced to give:[8]

$$\{u(t)\} = \sum_r \{u_r(t)\} = \sum_r X_r(t)\{\phi_r\}, \qquad r = 1, 2, \ldots, n \tag{59}$$

which represents the total displacement in terms of the generalized coordinates $X_r(t)$ of the uncoupled equations.

Mode superposition can now be summarized as consisting of four steps. The first calls for acquisition of the free-vibration frequencies and mode shapes, the second is the decoupling process which yields n single-degree-of-freedom equations, the third entails solution of the uncoupled equations in time to yield the generalized modal coordinates, and the fourth is the superpositioning of modal responses to obtain the total system response.

The major advantage of the mode superposition technique is that it involves transient solution of only single-degree-of-freedom equations. However, the advantage is of reduced significance if the response in all n nodes is considered, as a complete eigensolution is necessary to obtain the modes. Consequently, mode superposition becomes most advantageous when the total response can be approximated by relatively few modal responses, or when the responses of only a few modes are of interest (as might be the case in combustion instability analysis). Only one disadvantage exists, that being the necessity for an eigensolution, which is, in general, a complicated process; but this disadvantage is eliminated in combustion instability analyses since the eigensolution is already necessary for instability prediction. Therefore mode superposition is seen to be ideally suited to applications of dynamic response analysis in solid propellant rocket motors.

The acoustic free-vibration problem, Eq. (33), has been shown to be analogous to the structural free-vibration problem, Eq. (37). With Eq. (54) resulting from the transformation of the structural stiffness and mass matrices, it is apparent that similar transformation of the fluid inertia and fluid compressibility matrices will result in a similar uncoupled system. Only damping is yet to be shown as analogous, and this will now be done through consideration of the uncoupled system of Eq. (56).

In structural problems when Rayleigh damping is assumed, the damping matrix is a linear combination of the mass and stiffness matrices, Eq. (55). This results in an uncoupled damping coefficient,[8]

$$C_r = 2\xi_r\omega_r \tag{60}$$

A definition of the damping ratio is found in Ref. 7:

$$\xi = \frac{\ell n(u_0/u_n)}{2\pi n} \tag{61}$$

By examining the single-degree-of-freedom response equation,[7]

$$u(t) = u_0 e^{-\xi\omega t}\cos\omega t \tag{62}$$

and comparing it to the equation representing the basic combustion instability problem,

$$p(t) = p_0 e^{\alpha t}\cos\omega t \tag{62a}$$

a very simple analogy is recognized,

$$\alpha = -\xi\omega \tag{63}$$

Thus the growth/decay constant α is seen to be related directly to the damping ratio by proportion of the natural circular frequency, and the analogy of the two problems is complete.

Analytical Model of the Pulse

Impulse loading is the simplest form of dynamic perturbation. Rectangular, triangular, and sine-wave impulse forms are illustrated in Fig. 1. Pulse time and peak amplitude define the loading in each case, making the mathematical models of each type of impulse straightforward. Discharging of the pulse into a burning rocket motor cavity is equivalent to striking a structure with an impact load. The analytical pulse model is

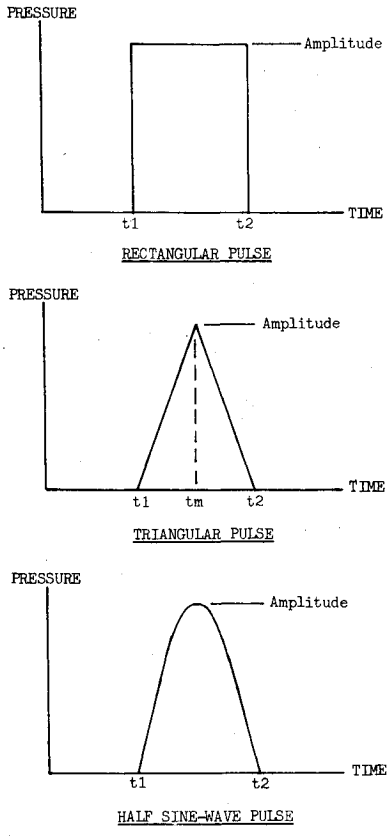

Fig. 1 Pulse diagrams.

applied in mode superpositioning by pulsing the appropriate nodal points of the discrete finite-element mesh, and then transforming the pulse into the contribution factor for each mode of interest. This transformation was defined in Eq. (57). Here the forcing function $\{f(t)\}$ is the pulse model described earlier and is a vector having nonzero values only at the nodes to be pulsed.

Developed Computer Code

Algorithms

The fundamental algorithm of the developed computer code is based on solution of the uncoupled acoustic vibration problem. As the theoretical development led to a direct analogy between structural and acoustic mode superposition problems, Eq. (56) can now be written in the form:

$$\ddot{X}_r - 2\alpha_r \dot{X}_r + \omega^2 X_r = \tilde{f}_r \tag{64}$$

Solution of Eq. (64) in time for each of the r modes yields time histories of the modal contribution factors, X_r. Integration of Eq. (64) in time is accomplished by applying the Newmark time-step integration algorithm,[8] which is an extension of the linear acceleration method. Adaptation to terminology used herein results in the two equations

$$\dot{X}_{t+dt} = \dot{X}_t + \left[(1-\zeta)\ddot{X}_t + \zeta \ddot{X}_{t+dt}\right] dt \tag{65}$$

$$X_{t+dt} = X_t + \dot{X}_t\, dt + \left[\left(\tfrac{1}{2}-\eta\right)\ddot{X}_t + \eta \ddot{X}_{t+dt}\right] dt^2 \tag{66}$$

where X_t (and its time derivatives) is the rth modal contribution factor, as before. Also utilized in the algorithm is the fundamental balance equation written at time $t + dt$,

$$\ddot{X}_{t+dt} - 2\alpha \dot{X}_{t+dt} + \omega^2 X_{t+dt} = \tilde{f}_{t+dt} \tag{67}$$

Rearrangement and solution of Eq. (66) for $\ddot{X}_{t+dt}$ in terms of X_{t+dt}, substitution of this expression into Eq. (65), and solution of Eq. (65) for $\dot{X}_{t+dt}$ in terms of X_{t+dt} yields expressions which may be applied to Eq. (67) to express it in terms of the unknown contribution factors X_{t+dt} only. The solution of Eq. (67) is then simple algebra, since it is a single linear equation of one unknown. Once the value of X_{t+dt} is known, it can be substituted back into Eqs. (65) and (66) to yield $\dot{X}_{t+dt}$ and $\ddot{X}_{t+dt}$.

The next significant algorithm is the superpositioning of the modal time histories to obtain the global time history of the pressure variation produced by the pulse. This superpositioning was defined in Eq. (59). Finally, the pulse algorithm is easily understood by referring once again to Fig. 1. Rectangular pulses are simply defined by the expression

$$p(t) = (\text{Amplitude})\Big|_{t1}^{t2} \tag{68}$$

Triangular pulses are expressed as

$$p(t) = (\text{Amplitude})\left(\frac{t-t1}{tm-t1}\right)\Big|_{t1}^{tm} \tag{69a}$$

$$p(t) = (\text{Amplitude})\left(\frac{t2-t}{t2-tm}\right)\Big|_{tm}^{t2} \tag{69b}$$

And half sine-wave pulses can be represented by

$$p(t) = (\text{Amplitude})\sin\left[\left(\frac{t-t1}{t2-t1}\right)\pi\right]\Big|_{t1}^{t2} \tag{70}$$

Thus the four major algorithms employed are defined and the program structure can now be discussed.

Program Structure

DRAMS (Dynamic Response Analysis by Mode Superposition) is developed in three units, the main program and two subroutines. Figure 2 illustrates the logic in flowchart form. The arrangement and function of each unit will be presented.

The main program begins execution with the input of data. Run control data is input and echoed, pulse data is then input and echoed, then the modal data, and finally, if called for by the problem definition, nonzero initial conditions are input. Next is the initialization process, whereby all variables are

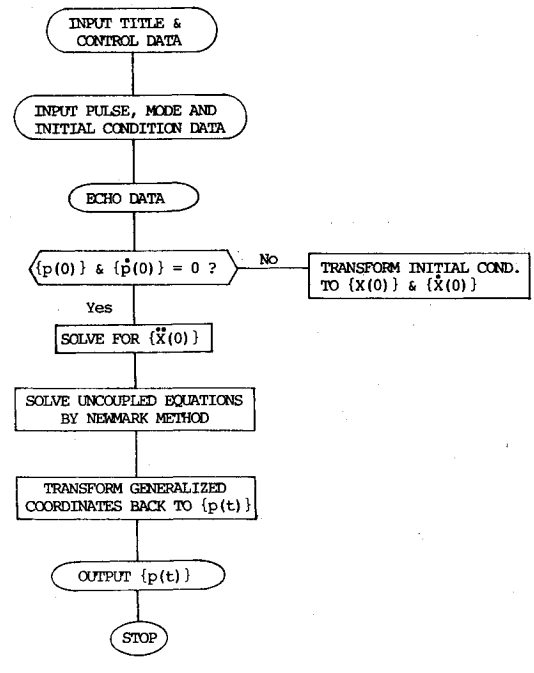

Fig. 2 DRAMS flowchart.

initialized and initial accelerations are calculated to provide all the values required by the Newmark time-step integration algorithm. These initial accelerations are generated from the solution of Eq. (64) at time zero for each mode. The main program then calls subroutine NEWMRK, which solves Eq. (64) in time to generate time histories of each modal contribution factor X_r. When execution control returns to the main program, the superpositioning process and data output are all that remain. Superpositioning is accomplished with the application of Eq. (59). At each time step, the modal contribution factor multiplies its respective mode shape vector and is summed into the global response array. The global responses are then output for the designated nodal points. Dummy counters are used to scan through the nodal point numbers to select those which are to have results output.

The main program is used primarily as a bookkeeper, whereas most computation is done in the two subroutines. The bookkeeping includes keeping track of the nodal point numbers of the discrete system solved, the nodal point numbers to be pulsed, and the nodal point numbers where solutions are sought, as well as the number of modal responses and time steps to be considered. After initializing global and modal force vectors, subroutine FORCE branches to the appropriate pulse type: rectangular, triangular, or half sine-wave. A pressure is calculated and this value is assigned to the global force vector at the appropriate pulse nodes. Finally, the global force vector is transformed through Eq. (57) into modal contribution factors $\tilde{f}_r$ before control is returned to the calling routine. Subroutine FORCE is called by subroutine NEWMRK at each time step.

Subroutine NEWMRK implements Eqs. (65), (66), and (67) to accomplish Newmark time-step integration. The first step is to calculate all necessary integration constants; there are seven generated when Eqs. (65) and (66) are rearranged in terms of X_{t+dt}. With constants assigned values, the time-step process begins. At each time step: subroutine FORCE is called to generate $\tilde{f}_r$'s, the transformed Eq. (67) is solved for X_{t+dt}, and Eqs. (65) and (66) are re-entered to generate $\dot{X}_{t+dt}$ and $\ddot{X}_{t+dt}$. After stepping through time in this loop process, NEWMRK returns control to the main program for superpositioning and output.

Example Problems

DRAMS was developed as a post-processor of eigensolution data. As it requires the natural circular frequencies, growth/decay constant, and mode shape vectors as input, it is ideally suited to process data generated by the FLAP3 three-dimensional combustion instability analysis program. FLAP3 generates the eigensolutions for various modes with harmonic regions of the solution space. A particular mode is therefore identified by its harmonic number and mode number. Example problems solved with DRAMS are run with data produced by FLAP3 analyses. Three runs are presented to demonstrate the capabilities of DRAMS and to illustrate the mode superposition technique.

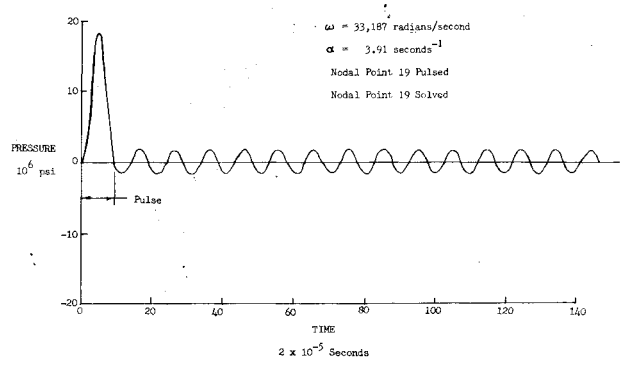

Fig. 3 Example 1.

The first analysis was conducted on Mode 2 (second longitudinal mode) of Harmonic 2, which was determined by FLAP3 to have a positive growth/decay factor. Recall that a positive factor indicates that a perturbation of that mode will produce oscillations with a growing amplitude. Figure 3 is a graphic representation of the analysis, and at first glance would seem to indicate no amplitude change. However, as the frequency of this example mode is 33,186.9 rad/s or 2068.3 Hz, and the growth/decay constant is only 3.91, an explanation of the lack of change is desirable. This explanation is best illustrated by returning to the structural analogy.

Structural damping was related to the growth/decay constant through the simple relationship of Eq. (63). As implied by its name, ξ is a ratio which relates modal damping factors to that mode's frequency. Structural frequencies are typically less than the frequency in this example's acoustic mode by approximately three orders of magnitude, and structural damping ratios are typically in the 5% to 10% range. The growth factor of 3.91 in this example, when compared to the frequency, is seen to be analogous to a damping ratio of 0.012%. These ratios are related to the amplitude change of the time history response from cycle to cycle, or from peak to peak, in Fig. 3. As the ratio in Example 1 is so small, no detectable change in amplitude would occur in as few cycles as are illustrated.

To emphasize this point and to demonstrate the time history capabilities of DRAMS, Example 2 was run with the same data as Example 1, except α was changed from 3.91 to 498.0. This new value represents a growth factor equivalent to a structural damping ratio of 1.5%. The amplitude growth evident in Fig. 4 clearly illustrates the instability problem, and though the growth rate of Example 1 was much smaller, at over 2000 Hz it would not take long to produce a more noticeable change.

Example 3 was run with data generated by a FLAP3 finite-element combustion instability analysis of a finocyl rocket motor. Five modes of the Zero Harmonic were analyzed to illustrate the superpositioning of modal responses and the responses which can be calculated at different nodal points within the cavity. Figure 5 is the graphic presentation of

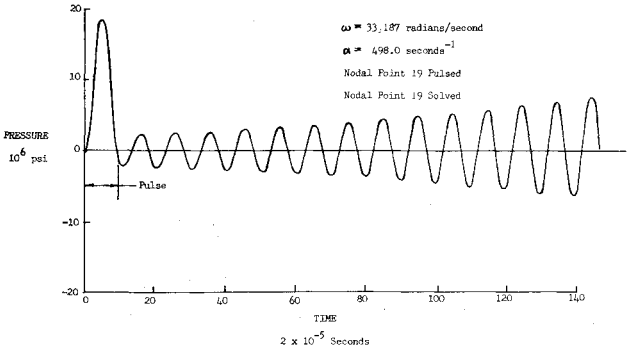

Fig. 4 Example 2.

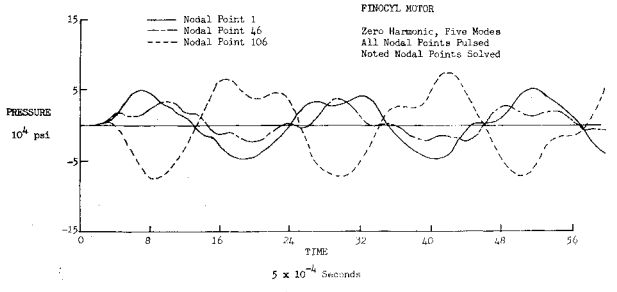

Fig. 5 Example 3.

Example 3. The response of any of the three nodal points recorded shows the effect of more than one mode's contribution, but the response of node 46 indicates superpositioning best. Also evident in this example is the value of the ability of DRAMS to examine response at several different nodal points, thereby indicating the most appropriate position for pressure transducer installation or pulse location.

The versatility of DRAMS as an analytical tool is evident. Example 1 shows that it can be used to model single mode analyses to examine the behavior of individually unstable modes. Example 2 illustrates that the analytical model can be altered by varying the parameters; this feature might be useful if the analytical frequency or the growth/decay constant varies from that determined experimentally. Through the insertion of experimental constants into the program along with a mathematically calculated mode shape, a more accurate overall model can perhaps be constructed. Finally, the superpositioning aspect illustrated with Example 3 shows that DRAMS has a capability to analyze the combined effects of several modes.

Results presented here are qualitative in nature; they are generated to illustrate specific aspects of mode superpositioning as a tool for the analytical pulsing of rocket motors.

Summary and Conclusions

Mode superposition has been shown to be ideally suited to the analytical modeling of solid propellant rocket motor pulsing. By developing a direct analogy between the acoustic free-vibration problem and the structural free-vibration problem, it has been shown that the mathematical models result in almost identical eigensystems. The solution of the acoustic eigensystem is necessary in linear combustion instability analysis, consequently mode shapes and frequencies for the acoustic system are available. A development of the theory of mode superposition in structural problems indicates that having mode shapes and frequencies, a system response can be found quite simply if the contributions of only a few modes are sought. This led to the final analogy between rocket motor acoustics and structural systems, that being the direct relationship between growth/decay constant α and damping ratio ξ. Inasmuch as the two problems are mathematically equivalent, the application of mode superposition is simply an extension of the finite-element method of discretized analysis.

Analytical modeling of experimental pulsing was chosen for two reasons. First, the pulse perturbation is the most easily modeled of any dynamic excitation. Second, the application of mode superposition to motor pulsing may be immediately beneficial. By "firing" analytical pulses at different locations within a cavity and recording the results, data could be generated which may increase the efficiency of the actual, much more expensive, experimental pulsing significantly. Nearly optimum locations for pulse injection and transducers may be obtainable.

This is not to say that mode superposition need be limited to the pulse testing of rocket motors. Should combustion research produce a reasonably accurate model of the actual propellant combustion, that model could be incorporated into a mode superposition analysis as the perturbation and perhaps eventually lead to the ability to model an entire motor burn cycle. An extensive analysis would, of course, be required, as the acoustic modal properties would change with the rocket motor configuration change due to consumption of the propellant, but it is feasible. A mode superposition program such as the one developed herein can easily accommodate any forcing function by simply substituting one "FORCE" subroutine for another.

It is hoped that this paper has presented the theory and application of mode superposition in an understandable manner. The intent of the authors is to show an analogy between two physical systems and to emphasize that the finite-element method is as applicable to one as it has been proven to be to the other. As a mathematical tool, finite-element analysis has opened the door to the discretization of many continuous systems. If this paper has encouraged the use of that tool, it has served its purpose well.

References

[1] Price, E.W., "Combustion Instability in Solid Propellant Rocket Motors," *Proceedings of the 9th International Astronautical Congress*, Amsterdam, Netherlands, Aug. 1958.

[2] Donn, J.J., Hewes, J.E., and Andrepont, W.C., "Solid Motor Pulsing for Evaluating Combustion Stability Characteristics," *Proceedings of the 13th JANNAF Combustion Meeting*, CPIA Publication 281, Vol. II, Sept. 1976, pp. 195-207.

[3] Baum, J.D., Lovine, R.L., and Levine, J.N., "Pulsing Techniques for Solid-Propellant Rocket Motors: Modeling and Cold-Flow Testing," *Journal of Spacecraft and Rockets*, Vol. 20, March-April 1983, pp. 150-157.

[4] Lovine, R.L., "Standardized Stability Prediction Method for Solid Rocket Motors," Vol. I, Aerojet Solid Propulsion Company, Sacramento, Calif., May 1976.

[5] Zienkiewicz, O.C., *The Finite Element Method*, 3rd ed., McGraw-Hill, Inc., New York, pp. 1-118, 135-177.

[6] Strang, G., *Linear Algebra and Its Applications*, 1st ed., Academic Press, Inc., New York, pp. 171-230.

[7] Clough, R.W. and Penzien, J., *Dynamics of Structures*, 1st ed. McGraw-Hill, Inc., New York, pp. 70, 191-202.

[8] Bathe, K.J. and Wilson, E.L., *Numerical Methods in Finite Element Analysis*, 1st ed., Prentice-Hall, Inc., Englewood Cliffs, N.J., pp. 308-344.

[9] Coates, R.L. and Horton, M.D., "Design Considerations for Combustion Stability," *Journal of Spacecraft and Rockets*, Vol. 6, Mar. 1969, pp. 296-302.

[10] Culick, F.E.C., Ed., "T-Burner Testing of Metalized Solid Propellants," Report No. AFRPL-TR-74-28, Air Force Rocket Propulsion Laboratory, Edwards AFB, Calif., Oct. 1974.

[11] Herting, D.N., "Acoustic Analysis of Solid Rocket Motor Cavities by a Finite Element Method," Report MS-116-2, The MacNeal-Schwendler Corporation, Los Angeles, Calif., May 1971.

[12] Hackett, R.M., "Three-Dimensional Acoustic Analysis of Solid Rocket Motor Cavities," *Technical Report RK-76-7*, U.S. Army Missile Research, Development and Engineering Laboratory, Redstone Arsenal, Ala., Nov. 1975.

[13] Hackett, R.M. and Juruf, R.S., "A Three-Dimensional Finite Element Code for Combustion Instability Prediction," *Proceedings of the 13th JANNAF Combustion Meeting*, CPIA Publication 281, Vol. II, Sept. 1976, pp. 267-280.

[14] Hackett, R.M. and Radke, R.R., "Acoustic Modeling and Combustion Instability Prediction with FLAP3," *Proceedings of the 14th JANNAF Combustion Meeting*, CPIA Publication 292, Vol. I, August 1977, pp. 91-98.

[15] Hackett, R.M., "Three-Dimensional Finite-Element Acoustic Analysis of Solid Rocket Motor Cavities," *Journal of Spacecraft and Rockets*, Vol. 13, Oct. 1976, pp. 585-588.